Efficient Light Management by Textured Nanoimprinted Layers for Perovskite Solar Cells

Marko Jošt,[†,¶,] Steve Albrecht,[¶,‡,*] Lukas Kegelmann,[¶] Christian M. Wolff,[§] Felix Lang,[¶] Benjamin Lipovšek,[†] Janez Krč,[†] Lars Korte,[¶] Dieter Neher,[§] Bernd Rech,[¶,¶] and Marko Topič[†]*

[†]University of Ljubljana, Faculty of Electrical Engineering, Tržaška cesta 25, 1000 Ljubljana, Slovenia

[¶]Helmholtz-Zentrum Berlin für Materialien und Energie GmbH, Institut für Silizium-Photovoltaik, Kekuléstraße 5, 12489 Berlin, Germany

[¶]Technische Universität Berlin, Fakultät IV - Elektrotechnik und Informatik, Marchstraße 23, 10587 Berlin, Germany

[‡]Helmholtz-Zentrum Berlin für Materialien und Energie GmbH, Young Investigator Group Perovskite Tandem Solar Cells, Kekuléstraße 5, 12489 Berlin, Germany

[§]University of Potsdam, Institute for Physics and Astronomy, Soft Matter Physics, Karl-Liebknecht-Str. 24-25,14476 Potsdam, Germany

*Email: marko.jost@fe.uni-lj.si
*Email: steve.albrecht@helmholtz-berlin.de

Abstract: Inorganic-organic perovskites like methylammonium-lead-iodide have proven to be an effective class of materials for fabricating efficient solar cells. To improve their performance, light management techniques using textured surfaces, similar to those used in

established solar cell technologies, should be considered. Here, we apply a light management foil created by UV nanoimprint lithography on the glass side of an inverted (p-i-n) perovskite solar cell with 16.3% efficiency. The obtained 1 mA cm^{-2} increase in the short-circuit current density translates to a relative improvement in cell performance of 5%, which results in a power conversion efficiency of 17.1%. Optical 3D simulations based on experimentally obtained parameters were used to support the experimental findings. A good match between the simulated and experimental data was obtained, validating the model. Optical simulations reveal that the main improvement in device performance is due to a reduction in total reflection and that relative improvement in the short-circuit current density of up to 10% is possible for large-area devices. Therefore, our results present the potential of light management foils for improving the device performance of perovskite solar cells and pave the way for further use of optical simulations in the field of perovskite solar cells.

Keywords: perovskite solar cells, anti-reflection, light management, UV nanoimprint lithography, optical simulations

The table of contents figure

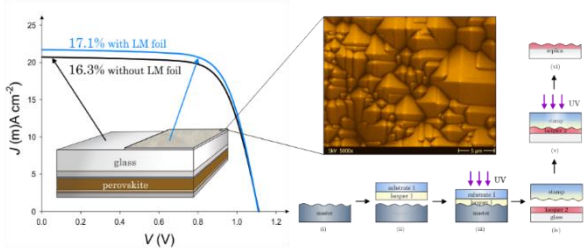

Recently, perovskites have emerged as a promising high-efficiency and low-cost absorber material in photovoltaics.[1–3] Extensive research has led to a fascinating progress and steep increase in conversion efficiencies. The record efficiency for mesostructured perovskite solar cell is currently set at 22.1%[4,5]. Due to lower processing temperatures, planar configurations

have also become popular, reaching efficiencies above 20% for both regular (n-i-p)[6] and inverted (p-i-n) configuration.[7–10] Especially the inverted structure has become an interesting solution as it is less prone to the detrimental *J-V* hysteresis and is also highly relevant for the tandem perovskite devices,[11,12] which is why we chose it in our study.

Besides material and process optimization, higher conversion efficiencies are possible by increasing light in-coupling using light management techniques. Anti-reflection (AR) and light trapping (LT) effects can be achieved by planar AR coatings (ARC) and/or textured interfaces between the different layers of the solar cell stack.[13] The planar ARC are usually flat and reduce the reflection by optimal thickness and refractive index grading of the layers at the interfaces (air/glass in our case). The textured interfaces can either be integrated inside the cell structure by texturing the front electrode, either the transparent conductive oxide[14] or charge transport material,[15–17] or by applying light management (LM) foils on the front glass side in a superstrate cell configuration.[18,19] Textured foils have advantage over the ARCs, especially in planar devices with flat interfaces, as besides reducing the reflection they can scatter (for nano-sized texture features) or refract (for micro-sized features) light, which prolongs the optical path. Using the LM foil, the light that is reflected from other layers in the stack is reflected back into the device from the inner walls of the pyramids, inducing light trapping.[20]As a result, the photocurrent density is enhanced. Especially for rather thin films, light trapping can maintain high photocurrent density and increase the open-circuit voltage due to enhanced carrier density as compared to thicker films with the same absorption properties.[21] In contrast to the texturing inside the device, the LM foil reduces the reflection and enables improving the device performance of already fabricated flat devices with no adjustments of the device fabrication procedures.

To create a transparent film with a desired texture for efficient light management UV Nanoimprint Lithography (UV NIL) can be used.[22–25] This is a replication process whereby

textures from a master can be transferred onto the substrate by imprinting viscous polymer films and curing them with UV light. Therefore, by using UV NIL an additional transparent textured layer with an arbitrary texture can be created on top of the cell, which enables light scattering and/or has AR properties. UV NIL is a simple, low-cost and low-energy procedure with high repeatability that is also suitable for large-area roll-to-roll manufacturing.

In this paper, we analyze the effects of light management in perovskite solar cells with the inverted structure. The textured light management (LM) foil was added to the front glass side of the device to reduce the reflection losses and enhance light trapping and consequently increase the short-circuit current density. The short-circuit current density (J_{SC}) is used as a measure to determine the improvement of solar cell performance. Results for devices, without and with the LM foil are compared, showing an improvement from 20.7 to 21.7 mA cm^{-2} (4.8% relative) in J_{SC} with the LM foil. 3D optical simulations based on experimentally obtained parameters are performed to provide further insight into the reasons for the improved performance. We establish that small area devices suffer from light escaping effect. Considering that, we find very good agreement between the experimental results and the simulations, which validates our optical model and opens possibilities for use of optical simulations in the optimization of perovskite solar cells.

To our knowledge there are only a few papers that report the use of light management foils in perovskite solar cells.[18,19,26] They all analyze small devices and do not predict the full potential of the LM foil. Also, no comprehensive experiment-versus-3D optical simulation study for inorganic-organic perovskite solar cells has been conducted yet, both without and with the light management (LM) foil. Here, the optical simulations are used to determine losses and potential light management improvements for large area devices (solar modules) that can be realized with perovskite solar cells with the front surface LM foil. For such large active area devices,

simulations reveal a relative boost of 10%. We also calculate V_{OC} increase due to enhanced charge carrier density at a thinner active layer.

Results and discussion

For the purpose of this study, we fabricated solution processed inverted (p-i-n) perovskite solar cells with the configuration glass/ITO/PTAA/$CH_3NH_3PbI_3$/PCBM/BCP/Ag as shown in Figure 1. This figure also contains a cross-section SEM image with each layer and its thickness labelled. To create a LM foil a UV NIL replication process was utilized following the steps as schematically shown in Figure 2a and described in detail in the experimental section. Briefly, a viscous lacquer deposited on a flexible substrate (ii) is imprinted on the textured master (i) and cured under UV light (iii). After separation, the so created stamp is used as a quasi-master and the process is repeated: the stamp (iv) is imprinted in the viscous replica lacquer deposited on the substrate and cured (v). The cured lacquer (replica) now has the exact same texture as the master (vi). A silicon wafer with <100> orientation, etched in KOH resulting in randomly distributed pyramids,[27,28] typical for wafer based silicon solar cells,[29] was used as a master. We chose this texture since it is known to have good anti-reflection and light trapping properties.[20] Additionally, randomly textured silicon wafers can be easily fabricated and replicated using the UV NIL process. Figure 2b shows an SEM image of the replica on a glass substrate. Randomly distributed pyramids with sharp peaks and edges as transferred from the master are clearly visible, confirming the success of the UV NIL replication process. Thin microscope glass slides were used as substrates for the replica, which was then fixed on the glass side of the devices using an index matching liquid.

The *J-V* measurements of the fabricated devices are presented in Figure 3a. The black lines represent results of a device without the LM foil and the blue lines for a device with the LM foil. To highlight the absence of pronounced hysteresis in our inverted devices, which agrees

well with other inverted device structures,[7,8,30] we performed *J-V* measurements using different scan directions, i.e. from J_{SC} to V_{OC} (forward scan, full lines) and from V_{OC} to J_{SC} (reverse scan, dashed lines), both obtained at a scan rate of 0.25 V s^{-1}. The biggest change between the devices is in J_{SC}. The *J-V* measurements reveal an increase in J_{SC} from 20.7 mA cm^{-2} to 21.7 mA cm^{-2}, which is a 4.8% relative improvement for the device with the LM foil. The high open-circuit voltage (V_{OC}) remained the same (1.11 V), while change in fill factor (FF) is negligible (70.9% to 71.2%). Overall, the power conversion efficiency (PCE) increases from 16.3% to 17.1%, which is a 5% relative improvement for the LM foil device over the flat device. A stabilized PCE of 16.1% for the device without the LM foil was obtained using maximum power point (MPP) tracking under operational conditions (Figure S4). This fits with the PCEs obtained in the reverse and forward scans. Table 1 lists the performance parameters of the devices without and with the LM foil. A similar comparison was carried out for the perovskite solar cells with PEDOT:PSS as a hole transporting material (Figure S1 and S2, Table S1). Again, the performance of the device was improved using the LM foil (relative improvement in J_{SC} is 8.6% and in PCE 7.9%).

Figure 3b shows the measured external quantum efficiency (EQE) (solid lines) and the total reflection spectra (dashed lines). The black lines represent the device without the LM foil and the blue lines with the LM foil. Two main regions of change can be identified in the spectra: The first region of differences is found in the wavelength range between 300 and 380 nm. Here, the EQE is lower when using the LM foil due to the absorption of UV light in the UV NIL layer. However, the relative contribution of the AM1.5G spectrum in this range is small and accounts for a current loss of only 0.08 mA cm^{-2}. The second region of differences is between 450 nm and 650 nm, in which the EQE increases significantly (compare also Figure 4b). This can be attributed to the reduced reflection of the incident light and improved light trapping as a consequence of the LM foil, as proven by reduction in total reflection in Figure 3b.

The LM foil reduces the total reflection (*R*) significantly across the whole wavelength range. The reflection of the cell stack with the LM foil over the high EQE plateau between 400 and 700 nm is on average more than 50% lower. The positions of the peaks and valleys in the *R* and EQE spectra match well for both cases, without and with the LM foil. However, only at the wavelengths where the reduction in the reflection is the highest are then translated to the EQE increase in Figure 3b. In the visible light range (400 – 700 nm), the EQE and the *R* curves added together amount to more than 94%, indicating small optical parasitic losses in the hole and electron transporting materials and the contact layers, and good extraction of the charge carriers. The sum of the EQE and *R* with the LM foil is slightly lower and we attribute this to refracted light escaping towards the sides of the device. The active area of the device (4 x 4 mm^2) is small compared to its thickness (including thick glass substrate – 1.1 mm) and also to the light spot of the EQE measurement setup (2.5 x 2.5 mm^2). Therefore, a significant portion of the incident light, when refracted into large angles, escapes from the device to substrate regions without electrodes. Photogenerated charges in these regions are not collected and consequently lost, resulting in lower EQE values.[31] This phenomenon is referred to as "escaped light" and is discussed in more detail below.

Table 1: Performance parameters, integrated J_{SC_EQE} from the EQE and equivalent J_{SC} loss from the reflection measurements R_{eq} of the fabricated solar cells without and with the LM foil. Relative changes are also shown.

	J_{SC} (mA cm^{-2})	J_{SC_EQE} (mA cm^{-2})	R_{EQ} (mA cm^{-2})	V_{OC} (V)	FF (%)	PCE (%)
Without LM foil, for.	20.7	20.5	6.63	1.11	70.9	16.3
Rev.	20.5			1.11	70.2	16.0
With LM foil, for.	21.7	20.7	4.37	1.11	71.2	17.1

	Rev.	21.6			1.11	70.3	16.8
Rel. change		+4.8%	+1%	-34%	0%	0%	+5%

By integrating the EQE spectra over the solar-spectrum, a relative increase in J_{SC_EQE} up to 1% is calculated (Table 1). The integrated EQE agrees well with the J_{SC} from the *J-V* measurement for the device without the LM foil, proving the accuracy of the measurements. The value for the device with the LM foil is, however, lower compared to that obtained by the *J-V* measurement. As mentioned before, this is attributed to the small device area and different illumination areas in EQE and *J-V* measurements. Equivalent reflection current loss (R_{EQ}), obtained by integrating the reflectance spectrum over the solar-spectrum, reveals that with the LM foil 34% less current is lost due to reflection when using the LM foil. Ideally, for large area devices most of the 2.2 mA cm^{-2} gained by reducing reflection would be converted to useful current. The difference to the 0.2 mA cm^{-2} gained in the EQE measurement is attributed to the escaped light. However, the gain of 1 mA cm^{-2} in the case of illumination with an area larger than the active solar cell area (*J-V* measurement) is more realistic to real module application due to the balance of light scattered into and outside of the active area.

In order to reveal the differences between the enhancement measured in EQE and J_{SC} as well as to provide an insight into the changes in optical loss distribution with the LM foil, we perform 3D optical simulations using the optical simulator CROWM.[31–33]. The simulator is based on combined ray and wave optics models that enable simultaneous simulations of both segments of the device, textured thick LM foil (incoherent light propagation) and thin-film solar cell stack (coherent light propagation). Using optical simulations, it is possible to establish how further improvements in J_{SC} can be achieved and if the LM foil is beneficial even for the highest performing devices. The thicknesses of the individual layers used in simulations are estimated from the cross-section SEM image and are 140 nm for ITO, 5 nm for PTAA, 270 nm

for the perovskite absorber, 50 nm for PCBM, 5 nm for BCP and 100 nm for Ag as shown in Figure 1. The fabricated solar cells also exhibit low roughnesses which enable successful matching with our simulations that assume planar interfaces. The wavelength-dependent *n* and *k* data needed to conduct the simulations were extracted from reflectance / transmittance (RT) data using optical modelling[34] and from the literature for the perovskite absorber.[35]. When simulating devices with the LM foil, we set the thickness of the LM foil to 50 μm and apply texture profile on the front surface. To include a realistic texture in the simulator, the texture profile of the random pyramids was measured using AFM (data not shown).

To validate the optical model, both the device area and the illumination beam size were set to the actual experimental values, which is necessary to get comparable results. Such case in which the realistic geometrical dimensions are taken into account is referred to as a "confined" device. The comparison between measured (black lines) and simulated (blue lines) EQE / absorptance (*A*) and *R* is presented in Figure 4a and b. It is assumed that all the absorbed photons result in charges that can be collected under short circuit conditions[36] and is proven by the good match between the measured EQE and *A* (solid lines). A good match is also obtained between the *R* curves (dashed lines) for both cases, without and with the LM foil. There are, however, slight discrepancies in terms of shape and values due to interferences (at 580 and 650 nm) from the thin layers, which are slightly less pronounced in the measurements. This is due to a slight roughness of the perovskite absorber that reduces interferences within the device while simulations assume planar interfaces. In the case of the LM foil, the textured front surface reduces interferences due to the refracted light beams now having different optical paths, thus also losing constant phase difference. Consequently, interference peaks are diminished and the simulation compares better to the experiment. Comparing the simulated integrated absorption spectra J_{SC_SIM}, the increase is from 20.5 mA cm^2 for the flat device to 21.1 mA cm^{-2} for the confined device with the LM foil, which is similar to the measured values. Similarly, the

analyzed solar cell devices with PEDOT:PSS as the hole transporting material, including detailed optical simulations, are presented in the supporting information in Figure S3. Again, there is a good match between experiments and simulations. Following this results, we believe that our optical simulations describe our system well therefore validating the optical model and making it first successful perovskite experiment-versus-simulation study conducted. Since the results are based on experimentally obtained parameters, the optical model can be used for further analysis, as well as for other device structures, configurations and texture optimization.

First, we investigate the expected improvements for large devices, relevant for practical applications in solar modules. Since such devices are much larger than our test device, it is now assumed in the simulations that the active area has infinite lateral dimensions in both directions and refer to this as an "unconfined" device. Keeping all the other input parameters the same, the increase in simulated current J_{SC_SIM} due to the LM foil is 11.2% (22.8 mA cm^{-2}). This means that the large area devices would benefit more from the LM foil than the test device. The *A* and *R* curves are plotted in Figure 4b with dark red lines. The simulations show the largest increase in the region around 580 nm. This is also where the highest increase in the EQE was measured. Additionally, compared to the confined case, there is an increase in the absorption for the longer wavelengths that is typical for other solar cell types. In the unconfined case, the longer wavelengths have more passes through the active layer and are thus more likely to be absorbed while for the confined/experimental case a high amount of long wavelength light leaves the active area before being absorbed. The *R* spectra for the unconfined and confined case are very similar, the *A* is, however, lower for the confined device over the whole spectrum. This confirms our conclusion from the EQE study that in small devices a high amount of light escapes the device area due to the refractions in the LM foil. Most of this refracted light escapes the device area already in the glass substrate due to its relative large thickness (1.1 mm) compared to the device's active area (see also Figure S6). For comparison,

Figure S5 and Table S2 show results for a device fabricated on a thinner substrate (0.7 mm). Overall, this device performs slightly worse, however, the increase in the EQE is higher due to the increased amount of light reaching the perovskite absorber and not exiting the cell. To fully harvest the improvements of the LM foil, a device with around 10 times bigger area is needed for the same beam spot (Figure S7).

Figure 5a displays the absorption spectra of the individual layers for the (unconfined) device without and with the LM foil. Most of the incident light is absorbed in the perovskite absorber while the main parasitic loss can be attributed to the total reflection and absorption of the layers located above the perovskite in the UV and blue spectrum. The LM foil reduces the reflection over the whole analyzed spectrum. Similarly to the experimental results presented above, the simulated equivalent reflection current loss R_{SIM} is reduced by almost 50%. Most of the gained in-coupled light contributes to the useful current in the absorbing perovskite layer, with an increase in the simulated photocurrent of 11.2%. The additional absorption due to the LM foil in the other layers is negligible. The solar-spectrum wavelength integrated absorptances of all the layers are shown in Table 2, while Figure S6 compares losses between confined and unconfined device. No pronounced difference other than the escaped light can be observed.

Table 2: Simulated current J_{SC_SIM} [mA cm^{-2}] that is produced in the perovskite absorber layer, lost as parasitic absorption in the other layers, or lost via reflection under AM 1.5G illumination for an unconfined device for the thicknesses as stated in Figure 1. The spectra for these two cases are presented in Figure 5a.

Texture	Reflection, R_{SIM}	ITO	PTAA	Perovskite, J_{SC_SIM}	PCBM	Ag
Flat	5.79	0.44	0.07	20.5	0.16	0.22
LM foil	3.24	0.50	0.08	22.8	0.16	0.30
Change	- 2.55	+ 0.06	+ 0.01	+2.3 (11%)	+ 0	+ 0.08

Second, the J_{SC_SIM} enhancement due to the LM foil was also determined for devices with different layer thicknesses. These devices might benefit less or not at all since the effect of the prolonged optical path of the oblique light beams after refraction at the front surface might be negligible due to the thicker absorber. Figure 5b shows J_{SC_SIM} (solid lines) and R_{SIM} (dashed lines) for perovskite layer thicknesses between 50 nm and 1000 nm without (black) and with the LM foil (blue). The dark red line shows the relative enhancement and the vertical dashed line the case for the perovskite absorber thickness of 270 nm investigated above. The J_{SC_SIM} increases only slowly for perovskite thicknesses above 700 nm in both cases, without and with the LM foil. A small interference effect is observable, which diminishes with increasing thickness of the perovskite absorber. The J_{SC_SIM} increases with the LM foil for all thicknesses of the absorbing layer. Thus, even devices that have a very thick perovskite absorber layers generating a very high photocurrent should benefit using the LM foil. For example, a device with a 1 μm thick perovskite absorber still shows a 1.7 mA cm^{-2} (7.8% relative) benefit from the LM foil. This is the case because the reduction in reflection and light trapping in the layers above the perovskite absorber remain regardless of the absorber thickness. The usage of the LM foil is therefore also beneficial for thick devices.

Finally, we calculate the potential theoretical increase in V_{OC} due to the higher carrier density. This can be achieved when using the LM foil to create the same amount of photocurrent at significantly reduced active layer thickness, thereby enhancing the generated carrier density.[21] Since V_{OC} is affected by generation and recombination, an enhanced generation rate (the same number of charges per smaller volume) has the potential to enhance the V_{OC}. Using the equations and parameters presented by Leijtens et al.,[21] where they show how the recombination dynamics of perovskite solar cells is dominated by long lived holes and trapped electrons with strongly reduced trap mediated recombination (electron lifetime: τ_n = 100 ns, long lived hole lifetime: τ_p = 10 μs), we calculate a potential V_{OC} increase of 36 mV (see SI for

more information). Here, the current is kept constant (20 mA cm^{-2}) but the thickness is changed to achieve such current – 130 nm in the case with the LM foil and 260 nm in the case without the LM foil (denoted with the crosses in Figure 5b). This indicates another potential benefit of the LM foil – besides increasing the J_{SC}, the V_{OC} can also be enhanced by using thinner active layers to enhance the charge carrier density.

Conclusion

In summary, we have presented and analyzed a light management option for perovskite solar cells, using a UV Nanoimprint Lithography process to fabricate a light management (LM) foil. Inverted perovskite solar cells (p-i-n) with an efficiency of 16.3% and negligible hysteresis have been fabricated to test the effect of the LM foil. The measurements with the LM foil reveal an increase in efficiency to 17.1%, which represents a 5% relative enhancement. The improvement in the performance can be contributed mainly to the increase in the short-circuit current of 4.8% %, as determined from *J-V* measurements.

Optical simulations based on experimentally obtained layer thicknesses and optical constants (*n*, *k*) show a good match with the experimental measurements for both cases, without and with the LM foil. These simulations confirm the experimental findings and validate the optical model for perovskite based solar cells. This makes optical simulations a powerful tool and paves the way for further investigation and optimization of the perovskite based solar cells and different possible textures of the LM foil.

We find that smaller area devices suffer from light escaping the active area which was confirmed and evaluated using optical simulations. The effect of confinement between illuminated and active area was analyzed and we find that the difference in EQE between simulation and experiment for devices with the LM foil could be attributed to a high amount of the refracted light not reaching the absorber, contributing to a lower EQE. In general, a

relative boost in photocurrent of ca. 8% is feasible for large area devices, even for active layers thicker than 1 µm. Additionally, simulations revealed that optimized light management can be used to reduce the thickness of the active layer to reduce the amount of absorber material and enhance the photogenerated density, resulting in an expected 36 mV enhancement of the V_{OC} at an identical photocurrent.

This study demonstrates the beneficial role of the LM foil in reducing reflection and increasing absorption in perovskite absorber, making the LM foil a promising solution for improving the performance of perovskite based solar cell.

Methods

Perovskite solar cell preparation. The fabricated perovskite solar cell devices have an inverted (p-i-n) planar structure and a layer configuration of glass/ITO/PTAA/$CH_3NH_3PbI_3$/PCBM/BCP/Ag. The PTAA is poly [bis (4-phenyl) (2,5,6-trimentlyphenyl) amine], PCBM is [6,6]-phenyl-C61-butyric acid methyl ester and BCP is bathocuproine. Patterned ITO coated glass (Lumtec, R = 15 Ω sq^{-1}) was used as a substrate, with the size of the individual active area being 4 x 4 mm^2. First, the substrates were sequentially cleaned in ultrasonic baths using an acetone, washing solution (Mucasol, 2%), H_2O and isopropanol, and then subjected to a 20 min UV-ozone treatment. All the layer deposition steps were conducted in a nitrogen atmosphere. The hole transport material PTAA (EM Index, Mw = 17.5 g mol^{-1}) was deposited using spin-coating (4000 rpm for 30 s) and annealed for 10 min at 100 °C. The perovskite was spun using one step solution process and crystallized at 80 °C for 5 min. The precursor solution was created from $PbAc_2$ (99.9%, Sigma Aldrich) and CH_3NH_3I (Dyesol) in 3:1 ratio, dissolved in anhydrous *N*,*N*-dimethylformamide (DMF, Sigma Aldrich) with a final concentration of 46 wt%. An appropriate amount of HPA was added to produce a 0.2% concentrated perovskite solution. Before perovskite spin-coating

a pure DMF spin coating step was utilized to enable better wetting of the perovskite on the PTAA surface[37]. The PCBM (Solenne, purity = 99.5%) was dissolved in anhydrous chlorobenzene (Sigma Aldrich) at a concentration of 20 mg ml^{-1}, spun at 1500 rpm for 1 min and annealed at 100 °C for 10 min. The BCP (Sigma Aldrich, purity = 99.99%) was dissolved in anhydrous ethanol (Sigma Aldrich) at a concentration of 0.5 mg ml^{-1}, spun at 4000 rpm for 1 min and annealed at 70 °C for 15 min. Finally, 100 nm Ag was deposited by thermal evaporation (10^{-7} mbar base pressure, 1 Å s^{-1}) to form the back contact.

UV NIL replication process. The UV NIL process was carried out in air following the steps as schematically shown in Figure 2a. A textured sample (i) is used as a master for the replication. A stamp lacquer, deposited on a substrate (ii), is imprinted on the textured master. Viscous lacquer adjusts to the structure of the master and is cured under UV light (iii). After the separation of the stamp from the master, the stamp can be used as a (quasi)master and is imprinted in the lacquer 2 (iv) that is deposited on the substrate. UV illumination cures the second lacquer (v). Once separated from the stamp, the acquired replica (vi) is ready for use as a light management foil. The created replica was fixed on the glass side using an index matching liquid (Norland Products Inc.). A silicon wafer with <100> orientation, etched in KOH with up to 8 μm resulting randomly distributed pyramids,[28,38] was used as a master. Hostaphan PET film and thin microscope glass lid were used as substrates for the stamp and the replica, respectively. Commercially available lacquers (provided by CCoatings) were used and deposited on the substrates using the doctor blade technique - the thickness of the layer before the imprint was 50 μm. UV LEDs with a peak wavelength at λ = 368 nm were used to cure the lacquers (t = 5 min). The refractive index of the cured replica (lacquer 2) is n = 1.55 which is close to the refractive index of the glass.

Device characterization. The current density–voltage (J-V) curve was measured using a Keithley 2400 Source Meter Unit in inert atmosphere under the illumination of simulated

AM 1.5G solar light from an Oriel class ABB solar simulator system, adjusted with a calibrated silicon reference cell (Fraunhofer ISE). The scan rate was 0.25 V s^{-1} with a voltage step of 20 mV. Note that the solar cells were measured without the use of an aperture mask to account for light scattered in and out of the active areas as denoted in the text. However, the good agreement between the integrated EQE spectra and the J_{SC} measured with unmasked devices ensures a good solar simulator and active area calibration and the absence of any edging effects. The external quantum efficiency (EQE) was measured as a function of wavelength from 300 to 850 nm with a step of 10 nm using an Oriel Instrument's QEPVSI-b system with 300 W Xenon arc lamp, controlled by TracQ™-Basic software. The illumination beam size of the EQE setup is 2.5 x 2.5 mm^2. The external quantum efficiency was measured without background illumination or applied bias voltage in inert atmosphere. The integrated EQE was in good agreement with J_{SC} from *J-V*. Reflection was measured as a function of wavelength from 300 to 850 nm with a step of 5 nm using an integrating sphere with a Perkin Elmer Lambda – 1050 UV/VIS/NIR spectrophotometer, calibrated with a white Spectralon. The illumination beam size of this setup is 3.5 x 3.5 mm^2

Optical simulations. 3D Optical simulator CROWM which is based on combined ray and wave optics model was used to conduct optical simulations. Wave optics model, based on transfer matrix algorithm, is used to simulate the thin layers (coherent light propagation) in the solar cell stack, while non-coherent ray tracing approach is used for thick layers (> 1 μm) – in this case the glass substrate and the LM foil. The wavelength-dependent *n* and *k* data needed to conduct the simulations were obtained using reflectance / transmittance (RT) method and from the literature for the perovskite absorber.[35] The main outputs of the simulator are total reflectance, transmittance and absorptance in each layer. Their solar-spectrum wavelength integration equals to the J_{SC} or equivalent current loss in the individual layer. The simulations were carried out in the wavelength range from 350 to 800 nm which is a sufficient range for

the perovskite solar cells. To include a realistic texture in the simulator, the texture profile of the random pyramids was measured using AFM. x,y,z results were directly imported into CROWM.

Associated content

Supporting information includes additional measurement and simulation results of the solar cell presented in the manuscript and of a similar solar cell but with PEDOT:PSS as a hole transporting material.

The Supporting Information is available free of charge on the ACS Publications website at DOI:

Author Information

Corresponding Authors

*E-mail: marko.jost@fe.uni-lj.si

*E-mail: steve.albrecht@helmholtz-berlin.de

Notes

The authors declare no competing financial interest

Acknowledgements

The authors are grateful to Carola Klimm, Institute for Silicon Photovoltaics, HZB for performing SEM measurements. The authors acknowledge the financial support from the Slovenian Research Agency (program P2-0197). M.J. thanks the Slovenian Research Agency for his PhD funding and Slovenian Human Resources Development and Scholarship Fund for his research stay scholarship. Additional financial support was provided by the German Federal

Ministry of Education and Research (BMBF) within the research initiative "Materialforschung für die Energiewende" (grant no. 03SF0540), by the German Federal Ministry for Economic Affairs and Energy (BMWi) through the "PersiST" project (grant no. 0324037C), and by the Bavarian Ministry for Economics, Media, Energy and Technology through the joint project "Hi-ERN".

References

(1) Snaith, H. J. Perovskites: The Emergence of a New Era for Low-Cost, High-Efficiency Solar Cells. *J. Phys. Chem. Lett.* **2013**, *4*, 3623–3630.
(2) Green, M. A.; Ho-Baillie, A.; Snaith, H. J. The Emergence of Perovskite Solar Cells. *Nat. Photonics* **2014**, *8*, 506–514.
(3) Grätzel, M. The Light and Shade of Perovskite Solar Cells. *Nat. Mater.* **2014**, *13*, 838–842.
(4) efficiency_chart.jpg (4349×2456) http://www.nrel.gov/pv/assets/images/efficiency_chart.jpg (accessed Nov 4, 2016).
(5) Saliba, M.; Matsui, T.; Domanski, K.; Seo, J.-Y.; Ummadisingu, A.; Zakeeruddin, S. M.; Correa-Baena, J.-P.; Tress, W. R.; Abate, A.; Hagfeldt, A.; Grätzel, M. Incorporation of Rubidium Cations into Perovskite Solar Cells Improves Photovoltaic Performance. *Science* **2016**, aah5557.
(6) Anaraki, E. H.; Kermanpur, A.; Steier, L.; Domanski, K.; Matsui, T.; Tress, W.; Saliba, M.; Abate, A.; Grätzel, M.; Hagfeldt, A.; Correa-Baena, J.-P. Highly Efficient and Stable Planar Perovskite Solar Cells by Solution-Processed Tin Oxide. *Energy Environ. Sci.* **2016**, *9*, 3128–3134.
(7) Heo, J. H.; Han, H. J.; Kim, D.; Ahn, T. K.; Im, S. H. Hysteresis-Less Inverted CH3NH3PbI3 Planar Perovskite Hybrid Solar Cells with 18.1% Power Conversion Efficiency. *Energy Environ. Sci.* **2015**, *8*, 1602–1608.
(8) Wu, C.-G.; Chiang, C.-H.; Tseng, Z.-L.; Nazeeruddin, M. K.; Hagfeldt, A.; Grätzel, M. High Efficiency Stable Inverted Perovskite Solar Cells without Current Hysteresis. *Energy Environ. Sci.* **2015**, *8*, 2725–2733.
(9) Zhu, Z.; Bai, Y.; Liu, X.; Chueh, C.-C.; Yang, S.; Jen, A. K.-Y. Enhanced Efficiency and Stability of Inverted Perovskite Solar Cells Using Highly Crystalline SnO2 Nanocrystals as the Robust Electron-Transporting Layer. *Adv. Mater.* **2016**, *28*, 6478–6484.
(10) Wang, Q.; Dong, Q.; Li, T.; Gruverman, A.; Huang, J. Thin Insulating Tunneling Contacts for Efficient and Water-Resistant Perovskite Solar Cells. *Adv. Mater.* **2016**, *28*, 6734–6739.
(11) Eperon, G. E.; Leijtens, T.; Bush, K. A.; Prasanna, R.; Green, T.; Wang, J. T.-W.; McMeekin, D. P.; Volonakis, G.; Milot, R. L.; May, R.; Palmstrom, A.; Slotcavage, D. J.; Belisle, R. A.; Patel, J. B.; Parrott, E. S.; Sutton, R. J.; Ma, W.; Moghadam, F.; Conings, B.; Babayigit, A.; Boyen, H.-G.; Bent, S.; Giustino, F.; Herz, L. M.; Johnston, M. B.; McGehee, M. D.; Snaith, H. J. Perovskite-Perovskite Tandem Photovoltaics with Optimized Bandgaps. *Science* **2016**, aaf9717.
(12) Bush, K. A.; Palmstrom, A. F.; Yu, Z. J.; Boccard, M.; Cheacharoen, R.; Mailoa, J. P.; McMeekin, D. P.; Hoye, R. L. Z.; Bailie, C. D.; Leijtens, T.; Peters, I. M.; Minichetti,

M. C.; Rolston, N.; Prasanna, R.; Sofia, S.; Harwood, D.; Ma, W.; Moghadam, F.; Snaith, H. J.; Buonassisi, T.; Holman, Z. C.; Bent, S. F.; McGehee, M. D. 23.6%-Efficient Monolithic Perovskite/Silicon Tandem Solar Cells with Improved Stability. *Nat. Energy* **2017**, *2*, 17009.

(13) Krč, J.; Topič, M. *Optical Modeling and Simulation of Thin-Film Photovoltaic Devices*; CRC Press, 2013.

(14) Paetzold, U. W.; Qiu, W.; Finger, F.; Poortmans, J.; Cheyns, D. Development of Perovskite Solar Cells with Nanophotonic Front Electrodes for Improved Light Incoupling. In *Photovoltaic Specialist Conference (PVSC), 2015 IEEE 42nd*; 2015; pp. 1–3.

(15) Kang, S. M.; Jang, S.; Lee, J.-K.; Yoon, J.; Yoo, D.-E.; Lee, J.-W.; Choi, M.; Park, N.-G. Moth-Eye TiO_2 Layer for Improving Light Harvesting Efficiency in Perovskite Solar Cells. *Small* **2016**, *12*, 2443–2449.

(16) Pascoe, A. R.; Meyer, S.; Huang, W.; Li, W.; Benesperi, I.; Duffy, N. W.; Spiccia, L.; Bach, U.; Cheng, Y.-B. Enhancing the Optoelectronic Performance of Perovskite Solar Cells via a Textured CH3NH3PbI3 Morphology. *Adv. Funct. Mater.* **2016**, *26*, 1278–1285.

(17) Tang, M.; Zhou, L.; Gu, S.; Zhu, W.; Wang, Y.; Xu, J.; Deng, Z.; Yu, T.; Lu, Z.; Zhu, J. Fine-Tuning the Metallic Core-Shell Nanostructures for Plasmonic Perovskite Solar Cells. *Appl. Phys. Lett.* **2016**, *109*, 183901.

(18) Tavakoli, M. M.; Tsui, K.-H.; Zhang, Q.; He, J.; Yao, Y.; Li, D.; Fan, Z. Highly Efficient Flexible Perovskite Solar Cells with Antireflection and Self-Cleaning Nanostructures. *ACS Nano* **2015**, *9*, 10287–10295.

(19) Dudem, B.; Heo, J. H.; Leem, J. W.; Yu, J. S.; Im, S. H. CH3NH3PbI3 Planar Perovskite Solar Cells with Antireflection and Self-Cleaning Function Layers. *J. Mater. Chem. A* **2016**, *4*, 7573–7579.

(20) Campbell, P.; Green, M. A. Light Trapping Properties of Pyramidally Textured Surfaces. *J. Appl. Phys.* **1987**, *62*, 243–249.

(21) Leijtens, T.; Eperon, G. E.; Barker, A. J.; Grancini, G.; Zhang, W.; Ball, J. M.; Kandada, A. R. S.; Snaith, H. J.; Petrozza, A. Carrier Trapping and Recombination: The Role of Defect Physics in Enhancing the Open Circuit Voltage of Metal Halide Perovskite Solar Cells. *Energy Environ. Sci.* **2016**.

(22) Chou, S. Y.; Krauss, P. R.; Renstrom, P. J. Nanoimprint Lithography. *J. Vac. Sci. Technol. B* **1996**, *14*, 4129–4133.

(23) Escarré, J.; Battaglia, C.; Söderström, K.; Pahud, C.; Biron, R.; Cubero, O.; Haug, F.-J.; Ballif, C. UV Imprinting for Thin Film Solar Cell Application. *J. Opt.* **2012**, *14*, 024009.

(24) Meier, M.; Paetzold, U. W.; Ghosh, M.; van Erven, A. J. M. Nano-Imprint Lithography for Advanced Light Management Concepts in Multi-Junction Solar Cells. In *Photovoltaic Specialist Conference (PVSC), 2014 IEEE 40th*; 2014; pp. 2836–2838.

(25) Köppel, G.; Rech, B.; Becker, C. Sinusoidal Nanotextures for Light Management in Silicon Thin-Film Solar Cells. *Nanoscale* **2016**, *8*, 8722–8728.

(26) Wang, D.-L.; Cui, H.-J.; Hou, G.-J.; Zhu, Z.-G.; Yan, Q.-B.; Su, G. Highly Efficient Light Management for Perovskite Solar Cells. *Sci. Rep.* **2016**, *6*, 18922.

(27) Bean, K. E. Anisotropic Etching of Silicon. *IEEE Trans. Electron Devices* **1978**, *25*, 1185–1193.

(28) Zubel, I.; Barycka, I. Silicon Anisotropic Etching in Alkaline Solutions I. The Geometric Description of Figures Developed under Etching Si(100) in Various Solutions. *Sens. Actuators Phys.* **1998**, *70*, 250–259.

(29) Battaglia, C.; Cuevas, A.; Wolf, S. D. High-Efficiency Crystalline Silicon Solar Cells: Status and Perspectives. *Energy Environ. Sci.* **2016**, *9*, 1552–1576.

(30) Meng, L.; You, J.; Guo, T.-F.; Yang, Y. Recent Advances in the Inverted Planar Structure of Perovskite Solar Cells. *Acc. Chem. Res.* **2016**, *49*, 155–165.
(31) Lipovšek, B.; Čampa, A.; Guo, F.; Brabec, C. J.; Forberich, K.; Krč, J.; Topič, M. Detailed Optical Modelling and Light-Management of Thin-Film Organic Solar Cells with Consideration of Small-Area Effects. *Opt. Express* **2017**, *25*, A176–A190.
(32) Lipovšek, B.; Krč, J.; Topič, M. Optical Model for Thin-Film Photovoltaic Devices with Large Surface Textures at the Front Side. *Informacije MIDEM – J. Microelectron. Electron. Compon. Mater.* **2011**, *41*, 264–271.
(33) Lipovšek, B.; Krč, J.; Topič, M. Optimization of Microtextured Light-Management Films for Enhanced Light Trapping in Organic Solar Cells Under Perpendicular and Oblique Illumination Conditions. *IEEE J. Photovolt.* **2014**, *4*, 639–646.
(34) Čampa, A. NIKA - Model for Extracting Refractive Indices. In *Proceedings of the 48th International Conference on Microelectronics, Devices and Materials & the Workshop on Ceramic Microsystems*; Otočec, Slovenija, 2012.
(35) Löper, P.; Stuckelberger, M.; Niesen, B.; Werner, J.; Filipič, M.; Moon, S.-J.; Yum, J.-H.; Topič, M.; De Wolf, S.; Ballif, C. Complex Refractive Index Spectra of CH3NH3PbI3 Perovskite Thin Films Determined by Spectroscopic Ellipsometry and Spectrophotometry. *J. Phys. Chem. Lett.* **2015**, *6*, 66–71.
(36) Yang, B.; Dyck, O.; Poplawsky, J.; Keum, J.; Puretzky, A.; Das, S.; Ivanov, I.; Rouleau, C.; Duscher, G.; Geohegan, D.; Xiao, K. Perovskite Solar Cells with Near 100% Internal Quantum Efficiency Based on Large Single Crystalline Grains and Vertical Bulk Heterojunctions. *J. Am. Chem. Soc.* **2015**, *137*, 9210–9213.
(37) Chen, B.; Bai, Y.; Yu, Z.; Li, T.; Zheng, X.; Dong, Q.; Shen, L.; Boccard, M.; Gruverman, A.; Holman, Z.; Huang, J. Efficient Semitransparent Perovskite Solar Cells for 23.0%-Efficiency Perovskite/Silicon Four-Terminal Tandem Cells. *Adv. Energy Mater.* **2016**, *6*.
(38) Hylton, J. D.; Kinderman, R.; Burgers, A. R.; Sinke, W. C.; Bressers, P. M. M. C. Uniform Pyramid Formation on Alkaline-Etched Polished Monocrystalline (100) Silicon Wafers. *Prog. Photovolt. Res. Appl.* **1996**, *4*, 435–438.